Geophys. J. Int. (2005) **160,** 217–226 doi: 10.1111/j.1365-246X.2004.02465.x

Seismic versus aseismic deformation in Iran inferred from earthquakes and geodetic data

F. Masson,[1,*] J. Chéry,[1] D. Hatzfeld,[2] J. Martinod,[3] P. Vernant,[1] F. Tavakoli[4] and M. Ghafory-Ashtiani[5]

[1] *Laboratoire Dynamique de la Lithosphère, Université Montpellier II-CNRS, Pl. E. Bataillon,* 34095 *Montpellier Cedex* 05, *France*
[2] *Laboratoire de Géophysique Interne et Tectonophysique, Université Joseph Fourrier-CNRS,* BP 53, 38041 *Grenoble Cedex* 9, *France*
[3] *Laboratoire de Mécanismes de Transfert en Géologie, Université Paul Sabatier-CNRS, Rue des* 36 *Ponts,* 31400 *Toulouse, France*
[4] *Geodynamic Department, National Cartographic Center,* PO Box 13185-1684, *Meraj Ave., Tehran, Iran*
[5] *International Institute of Earthquake Engineering and Seismology, Farmanieh, Dibaji, Arghavan St.,* No 27, 19531 *Tehran, Iran*

Accepted 2004 August 25. Received 2004 July 30; in original form 2004 April 9

SUMMARY

A combined analysis of the geodetic strain-rate field and the strain-rate field deduced from the seismicity allows us to define the style of deformation and to distinguish seismic from aseismic deformation. We perform this analysis in Iran where the present-day tectonics results from the north–south convergence between the plates of Arabia to the south and Eurasia to the north. The data consist of velocities measured with a GPS network of 28 benchmarks and of instrumental and historical earthquake catalogues. The axes of the seismic strain-rate tensor have similar orientations to those deduced from the GPS velocity field. This indicates that the seismicity can be used to improve GPS information on the style and the orientation of the deformation. Comparison of seismic and geodetic strain rates indicates that highly strained zones experience mainly aseismic deformation in southern Iran and seismic deformation in northern Iran. A large contrast is observed between the Zagros (less than 5 per cent seismic deformation) and the Alborz–Kopet-Dag regions (more than 30–100 per cent seismic deformation). The distribution of the seismic/geodetic ratio correlates with the distribution of large earthquakes: intensive, low-magnitude seismicity is observed in the Zagros whereas the largest earthquakes occur in northern Iran. The contrast of seismic deformation between the Zagros and peri-Caspian mountains is confirmed considering 300 or 1000 yr of seismicity rather than 100 or 200 yr.

Key words: GPS, intracontinental deformation, Iran, seismicity.

1 INTRODUCTION

Geodetic strain and seismic deformation recorded over a few years are short-term geophysical measurements that allow one to define strain-rate tensors. It is tempting to use them to map geological strain rates. However, extrapolating short-term deformation to geological deformation runs serious risks. Because of the transient motion due to the seismic cycle, it is not always possible to directly use the geodetic strain to construct long-term strain. This problem appears to be critical along active faults where geodetic motion represents a smooth interseismic motion, not long-term motion that may display major discontinuities across faults. It is negligible if the GPS measurements are performed far from the active faults (50–100 km for a locking depth of 10 km). The strain deduced from earthquake focal mechanisms should also be used with care in order to get reliable geological information. Indeed, a few earthquakes recorded over a short period may not be representative of both strain direction and intensity over a much longer timescale. In addition aseismic deformation may take place, leading to a difference between geological and seismic strain. We present here a critical study of the geodetic and seismic strain of Iran with the aim of providing insights into the deformation process of this tectonically active zone.

Comparison of the seismic and geodetic deformation is important both for understanding geological deformation and for earthquake hazard assessment. Style, direction and rate can be compared. Because of the lack of common data sets, only a few studies combine geodetic and seismological strain analysis (Papazachos & Kiratzi 1992; Jackson *et al.* 1994; Shen-Tu *et al.* 1998; Kreemer *et al.* 2000; Jenny *et al.* 2004). By contrast, numerous studies of plate boundaries (Pacific–North America plate motion (Ward 1990; Shen-Tu *et al.* 1999), North Anatolian Fault (Straub *et al.* 1997; McClusky *et al.* 2000), Aegean domain (Armijo *et al.* 1999), Andes (Hindle *et al.* 2002)) have used geodetic observations alone to

* Corresponding author: Université Montpellier II, CC060, 4 place E. Bataillon, 34095 Montpellier Cedex 05, France. E-mail: fmasson@dstu.univ-montp2.fr

estimate the long-term deformation. However, this requires avoiding data that may have been contaminated by coseismic and post-seismic motion. Also, a seismic cycle model needs to be used in the fault vicinity in order to reconstruct the long term—geological—motion.

Obviously, only the seismic part of the strain-rate tensor is estimated from seismicity data. Its estimation strongly depends on the completeness of the instrumental seismicity catalogue. Although focal mechanisms and precise magnitudes have been systematically available since 1960–1970, this time interval is far too short to cover the recurrence time of most of the large earthquakes (McCaffrey 1997). There is a great likelihood that the amplitude of the seismic deformation in a region based on instrumental seismicity would either be significantly lower or larger than the real one (Kreemer *et al.* 2002). Therefore, the amplitude of the seismic deformation (i.e. the seismic strain rate) must be evaluated using both instrumental and historical catalogues. Then we are faced with the problem of the completeness and the quality of the historical seismicity catalogues.

Amelung & King (1997) showed that when averaged over a regional scale, the strain released by small earthquakes along the San Andreas Fault zone closely follows the regional pattern of tectonic deformation. If this finding has a general significance, this means that the style (i.e. normal, thrust or strike-slip) and the direction of the seismic strain-rate tensor could be determined using the instrumental seismicity catalogues. The style and direction of the seismic strain tensor have been used, for example by Kreemer *et al.* (2003), to create a global strain model. If the recurrence time of the earthquakes is smaller than the duration of the seismicity catalogue, the style and the direction of the geodetic deformation must be similar to the style and the direction of the seismic deformation except when the style and direction of the seismic deformation are different from the aseismic deformation. Conversely, if the style and direction are different, this may indicate that the duration of the earthquake catalogue is too short to cover the seismic cycle. This may also indicate that the earthquake catalogue covers only the recurrence interval of the small earthquakes and that the style and direction of the small and large earthquakes are different.

Bearing in mind the potential pitfalls of the common analysis of the geodetic and seismological data, it remains interesting to compare the seismic and geodetic strain rates and to compute the seismic/geodetic strain-rate ratio. This ratio should range in principle between 0 and 1 if the geodetic strain rate is not biased by co- and post-seismic deformation. If it is close to 1, most of the deformation is seismic. Conversely a low ratio shows an apparent seismic moment deficit. This could indicate either a large proportion of aseismic deformation or overdue earthquakes.

This paper is devoted to a comparison of seismic and geodetic deformation in Iran. Iran corresponds to a large intensely deforming area ($\sim 1500 \times 1500$ km^2) with various tectonic features (mountain ranges, stable blocks, large strike-slip fault zones). It is characterized by an intensive and well-known historical seismicity (Ambraseys & Melville 1982). Seismic hazard is one of the main problems of the country as shown by recent large earthquakes and seems geographically correlated to the seismic/total deformation ratio. Jackson & McKenzie (1988) have studied the deformation in Iran and quantified the seismic/total deformation ratio of the deforming zones of Iran. This ratio was based on a comparison of the seismic strain-rate tensor deduced from instrumental and historical seismicity and the total deformation deduced from plate movements. No geodetic data were available at this time. Because Iran is now covered by a GPS geodetic network (Nilforoushan *et al.* 2003; Vernant *et al.* 2004a), it is possible to compute the geodetic strain-rate tensor and to compare it with seismic strain-rate tensors. Three parameters (style, direction and rate) will be investigated. Because of the variety of error sources, defining real uncertainties for the GPS velocities is not a trivial problem, especially because only two surveys were conducted. This has been addressed in Vernant *et al.* (2004a) by using two sites in northwest Iran which were surveyed three times (DAMO and MIAN, surveyed in 1999, 2001, 2002). The velocities of DAMO and MIAN do not differ significantly using two surveys or three surveys, indicating that the uncertainties proposed by Vernant *et al.* (2004a) are probably reasonable.

The paper is organized as follows: after a short description of the tectonic context, we evaluate the geodetic and seismic strain-rate tensors. We compare the style and directions of the seismic and total deformation. We study the stability of the style and direction of the seismic deformation varying the interval of magnitude used. We calculate the seismic/total deformation ratio and evaluate its stability varying the time interval of the catalogue of historical seismicity. We finally discuss our results in term of crustal deformation processes.

2 TECTONIC CONTEXT

The present tectonics of Iran results from the north–south convergence between the plates of Arabia to the southwest and Eurasia to the northeast (Jackson & McKenzie 1984). It involves a juvenile continental collision (Falcon 1974; Berberian & King 1981) except along the Makran, its southeastern margin, where a remnant part of the Tethys oceanic lithosphere subducts northwards beneath southeast Iran (Byrne *et al.* 1992) (Fig. 1). Within Iran, most of the deformation is accommodated in the major belts (Zagros, Alborz, Kopet-Dag) and along large strike-slip faults which surround blocks (Central Iran, Lut and the southern Caspian Sea) with moderate relief and seismicity (Jackson & McKenzie 1984; Berberian & Yeats 1999).

A GPS network of 28 benchmarks was surveyed in September 1999 and October 2001 (Fig. 1) (Nilforoushan *et al.* 2003; Vernant

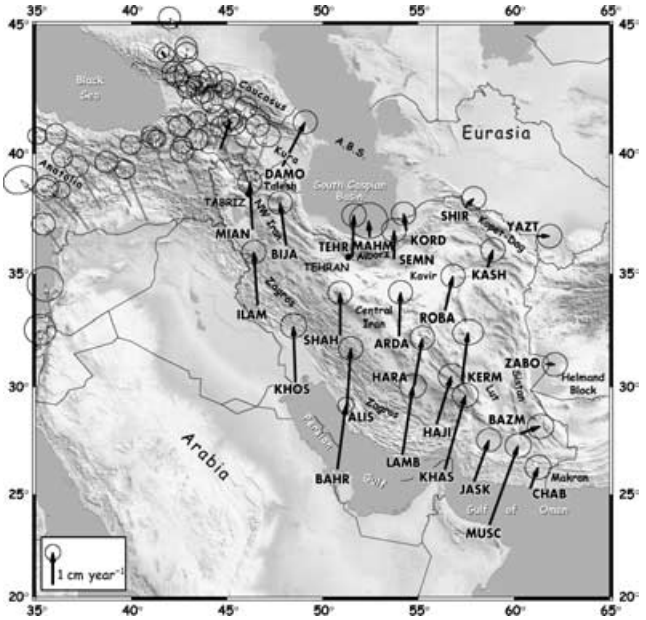

Figure 1. GPS horizontal velocities and their 95 per cent confidence ellipses superimposed on the topographic map of the studied area. GPS stations are indicated by capital letters, and major geological structures are labelled. Black arrows (Vernant *et al.* 2004a) and white arrows (McClusky *et al.* 2000) indicate the GPS velocities calculated in a Eurasia-fixed reference frame.

et al. 2004a). It complements several recent GPS studies of the deformation along the Alpine–Himalayan collision zone performed in China (Wang *et al.* 2001) and in the eastern Mediterranean and Caucasus area (McClusky *et al.* 2000). An expanded description and discussion of the velocity field has been given by Vernant *et al.* (2004a) and we present only a brief overview of the velocity field (Fig. 1). At the longitude of the Gulf of Oman, the north–south convergence rate between Arabia and Eurasia is 25 ± 2 mm yr^{-1}, trending N5°E. Benchmarks located east of Sistan (YAZT, ZABO) do not move significantly relative to Eurasia, which suggests that western Afghanistan (Helmand Block) is attached to Eurasia. Points MIAN, BIJA, SHAH and ARDA, located on the Central Iranian Block, consistently move to the north relative to Eurasia at a velocity of 14 ± 2 mm yr^{-1}. This confirms the rigidity of the Central Iranian Block (Jackson & McKenzie 1984) suggested by the lack of seismic activity (Fig. 2a). Most of the north–south shortening accommodated in western Iran concentrates in the two major mountain ranges, the Zagros and the Alborz/Caucasus, and on major active faults surrounding rigid blocks. The north–south shortening rate accommodated by the folded belt part of the Zagros range increases from 4 ± 2 mm yr^{-1} in its western part to 9 ± 2 mm yr^{-1} in its eastern part. To the north the transition between northwestern Iran (12 mm yr^{-1} trending 350°N in MIAN) and the Kura Basin (14 mm yr^{-1} trending 26°N in DAMO) is explained by large east–west strike-slip movements along the Tabriz Fault (Hessami *et al.* 2003; Masson *et al.* 2004). The Alborz range, located between central Iran (i.e. TEHR) and the South Caspian Basin (MAHM) shortens at a rate of 5 ± 2 mm yr^{-1} (Vernant *et al.* 2004b). Due to its narrowness, the Alborz range deforms more than Zagros. To the east, our measurements suggest that the subduction rate of the oceanic Arabian Plate beneath the Makran is 18 mm yr^{-1} to the east (MUSC–CHAB) and decreases to 15 mm yr^{-1} to the west (MUSC–JASK). A dextral shear of 14 ± 2 mm yr^{-1} occurs between the Helmand Block and the Central Iranian Block. To the south, the transition zone between Zagros and Makran is under transpression with a right lateral motion of about 11 ± 2 mm yr^{-1}. Sites located north of the Kopet-Dag (SHIR and YAZT) do not show rapid movement relative to Eurasia.

The 1964–1999 instrumental seismicity of Iran (Engdahl *et al.* 1998 Fig. 2a) is closely related to the deformation zones described above. Earthquakes occur mostly in the mountain ranges (Zagros, Alborz, Kopet-Dag), in northwest Iran and along the large faults surrounding the Central Iran and Lut blocks. With the notable exceptions of the Central Iran and Lut blocks, which are aseismic, Iran is characterized by intense seismicity. Nevertheless, the seismicity does not present the same characteristics everywhere. Plotting not only the number of events (Fig. 2a) but also the energy released by the earthquakes (Fig. 2b), a contrasted behaviour appears between the Zagros and the other seismic regions of Iran. The Zagros shows very intense but low-magnitude seismicity, but in the north, from the Turkish border to the Kopet-Dag, earthquakes are less frequent but with higher magnitudes. Jackson & McKenzie (1988) proposed that the Zagros suffers predominantly aseismic deformation while seismic deformation characterizes the Alborz and Kopet-Dag regions.

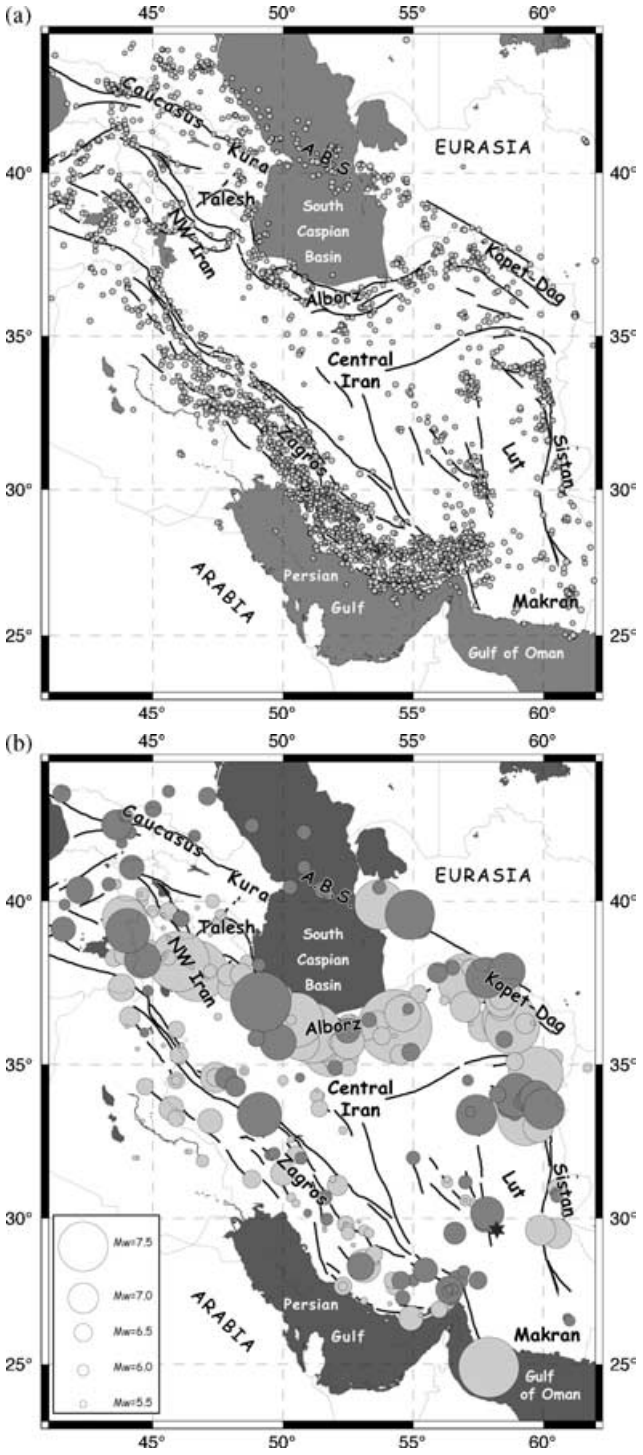

Figure 2. (a) Earthquake distribution in Iran from the instrumental seismicity catalogue (1964–1999, Engdahl *et al.* 1998). (b) Seismicity map of Iran amplifying the large earthquakes to provide a view of the released seismic energy. Dark grey, 1909–2002 seismicity from Jackson *et al.* (1995) and the Harvard catalogue. Light grey, historical seismicity (before 1909) from Ambraseys & Melville (1982). The star indicates the location of the recent Bam earthquake, not included in this study.

3 GEODETIC AND SEISMIC STRAIN-RATE TENSORS

3.1 Geodetic strain-rate tensor

Because of the large distance between most of the GPS sites and the large faults, we assume that the co- and post-seismic motion the location of benchmarks is negligible all along the seismic cycle. Therefore, it seems reasonable to assume that the geodetic strain rate represents the interseismic strain rates. Although this hypothesis is not necessary to compare seismic and geodetic strain, this would

imply that the geodetic strain rate is also equivalent to that averaged over geological time.

Under the hypothesis that the velocity field v varies linearly inside each triangular subnetwork spanning the GPS network, we calculate the average horizontal velocity gradient $L = \mathrm{grad}(v)$ over each triangle. Because the velocity gradient generally incorporates both deformation and rotation, this 2-D tensor is asymmetric. L can be separated in a symmetric and antisymmetric part as follows:

$$L = \frac{1}{2}(L + L^{\mathrm{T}}) + \frac{1}{2}(L - L^{\mathrm{T}}).$$

Its symmetric part is the strain-rate tensor while its antisymmetric part gives a local measure of the rate of rigid rotation (Malvern 1969). The strain rate calculated from the horizontal velocity field is shown in terms of their principal axes in Fig. 3(a) and in Table 1.

To the south, the Persian Gulf does not suffer deformation. Very high shortening rates are observed along the Makran subduction and in the Zagros–Makran transition zone. High strain rates are also observed in the Zagros and Alborz. These two orogens experience tranpressive strain of comparable amplitude. However, this similarity, due to the coarse sampling of the geodetic network (200 km), precludes the detection of a more pronounced strain peak of Alborz (Vernant *et al.* 2004b). A dominant strike-slip strain is found in the northwest Iran–Turkish zone and around the Lut Block.

To estimate the uncertainties of the geodetic strain rates, we focus on three triangles with small, medium and large geodetic strain rates (triangles 2, 4 and 24 respectively). For each triangle, we compute 100 strain-rate tensors introducing a normally distributed random variation of the velocities (Fig. 3b) based on the standard errors proposed by Vernant *et al.* (2004a). For the three triangles the direction and the amplitude of the strain have small standard deviations (less than 10° for the direction and less than 1×10^{-8} yr^{-1} for the strain rate).

3.2 Seismic strain-rate tensor

The method of analysis followed here is based on the formulation of Kostrov (1974) and Jackson & McKenzie (1988), already intensively used for example in the Mediterranean domain (Papazachos & Kiratzi 1992; Jackson *et al.* 1994) or in Asia (Holt *et al.* 1995). If the deformation that occurs within a volume V containing active faults is seismic, Kostrov (1974) shows that the average seismic strain rate $\dot{\varepsilon}_{ij}$ during a time t is:

$$\dot{\varepsilon}_{ij} = \frac{1}{2\mu t V} \sum_{n=1}^{N} M_{ij}^{n}$$

where μ is the modulus of rigidity and M_{ij}^{n} the components of the moment tensor M^{n} of earthquake n. M^{n} is defined from the scalar moment M_0^{n} and the unit vector normal to the fault plane and the unit vector in the direction of slip. We take $\mu = 3 \times 10^{10}$ Pa. Based on focal depth estimates obtained by waveform modelling, Jackson & McKenzie (1988) assumed a thickness of 15 km for the seismogenic layer in Iran. This has been confirmed by microseismic studies in the Zagros and the Alborz (Tatar 2001; Hatzfeld *et al.* 2003) or studies of focal mechanisms from teleseismic waves (Talebian & Jackson 2004) and we use this value to compute the volume V of each triangle defined with the GPS benchmark locations.

We compute a first estimation of the seismic strain rate for each triangle using the earthquake catalogue of Jackson *et al.* (1995) for the time period 1909–1991 completed for the time period 1992–2002 by the Harvard centroid moment tensor catalogue. We select all the events with a magnitude M_{w} (or M_{s} if M_{w} is unknown) greater

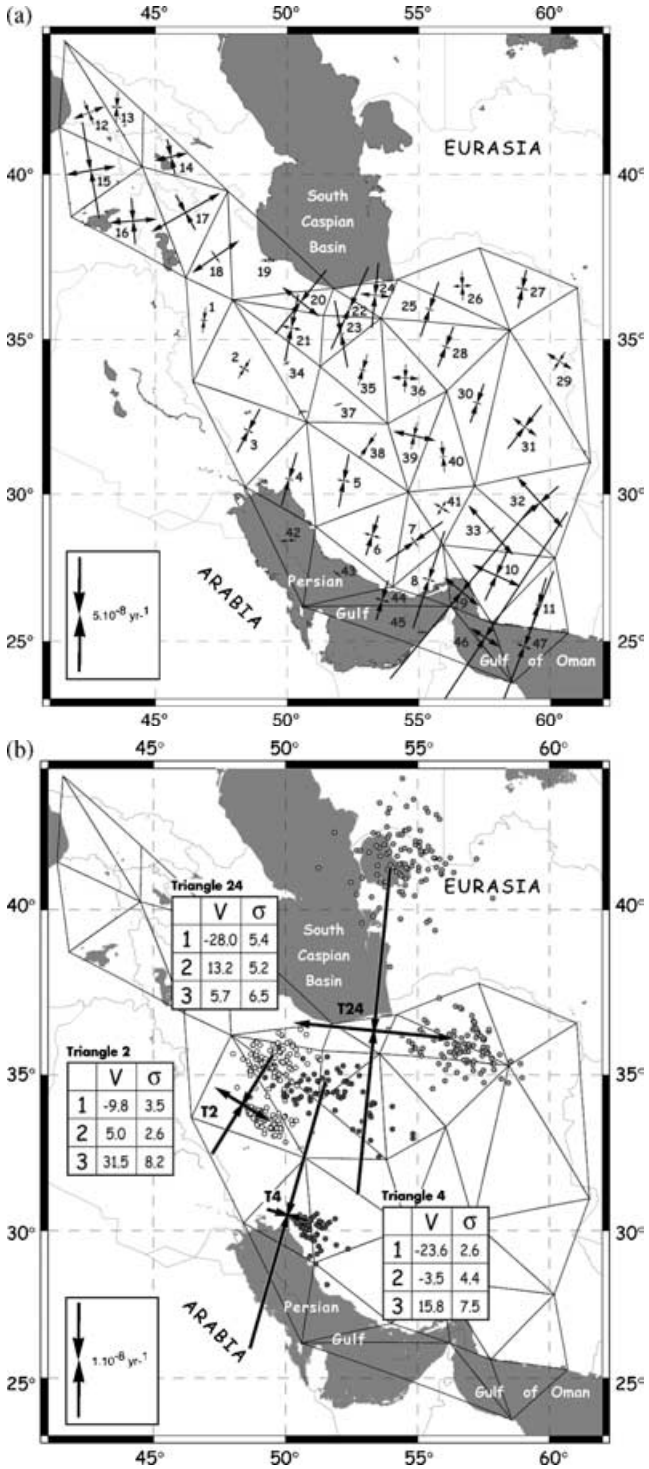

Figure 3. (a) Principal horizontal axes of the geodetic strain rate tensor obtained using the GPS velocity field of Fig. 1 and several velocities from McClusky *et al.* (2002). (b) Estimation of the uncertainties of the geodetic strain rates for triangles 2 (light grey), 4 (black) and 24 (dark grey) (see text for details on the computation). Dots indicate the location of the extremity of the arrows. In the tables 1 is the amplitude of axis 1 (multiplied by 10^9 in yr^{-1}), 2 is the amplitude of axis 2 (multiplied by 10^9 in yr^{-1}) and 3 is the azimuth of axis 1. The obtained value is in the first column and the estimated standard deviation in the second column.

Table 1. Geodetic and seismic strain for each triangle of Figs 3–7. Triangles are numbered and classified by tectonic region allowing the computation of mean strain: Tr = triangle, 1 = amplitude of the first axis of the strain tensor multiplied by 10^9 in yr^{-1} (compression for most of the triangles), 2 = amplitude of the second axis of the strain tensor multiplied by 10^9 in yr^{-1} (extension for most of the triangles), 3 = azimuth of the first axis, S/G = ratio of the seismic strain computed from focal mechanisms and magnitudes (database 1909–2002) to the geodetic strain, M_0/Geodetic = ratio of the seismic strain computed from magnitudes (database 1000–2002) to the geodetic strain, 100y = 100 yr, 200y = 200 yr, 300y = 300 yr, 1000cy = 1000 yr.

Tr.	Region	Long.	Lat.	Geodedic Strain			Seismic Strain			S/G	Mo/Geodetic			
				1	*2*	*3*	*1*	*2*	*3*	100y	100y	200y	300y	1000y
1	NW Zagros	46,84	35,6	-11,1	2,8	6,8	0,0	0,0		0%	0%	0%	0%	0%
2	NW Zagros	48,37	34,08	-9,8	5,0	31,5	-19,4	18,0	0,5	241%	184%	94%	63%	26%
	NW Zagros									171%	130%	67%	44%	19%
3	Zagros	48,53	32,09	-21,1	4,9	27,6	-0,5	0,0	39,7	2%	3%	1%	1%	0%
4	Zagros	50,08	30,51	-23,6	-3,5	15,8	-0,5	0,1	7,7	2%	3%	2%	1%	3%
5	Zagros	52,15	30,45	-23,0	5,9	10,8	-0,7	0,1	42,0	3%	3%	5%	3%	2%
6	Zagros	53,23	28,63	-17,8	7,5	17,2	-2,3	0,0	11,7	12%	12%	10%	6%	8%
7	Zagros	54,84	28,42	-29,6	-5,0	54,8	-6,7	0,0	176,6	22%	23%	11%	8%	4%
8	Zagros	55,38	27,13	-43,7	6,2	17,9	-1,6	0,0	0,0	4%	4%	4%	3%	1%
	Zagros									6%	7%	5%	3%	3%
9	Zagros-Makran	56,64	26,72	-96,4	19,9	39,5	-15,2	0,0	171,2	15%	16%	8%	5%	2%
	Zagros-Makran									15%	16%	8%	5%	2%
10	Makran	57,95	27,27	-23,5	22,4	24,4	-3,5	0,0	175,1	11%	11%	6%	4%	1%
11	Makran	59,55	26,27	-24,2	3,0	16,3	-0,8	0,8	6,3	4%	3%	2%	1%	0%
	Makran									8%	8%	4%	3%	1%
12	NW Iran/Caucasus	42,47	41,79	-11,3	14,2	158,2	-1,6	0,0	7,9	9%	9%	5%	3%	1%
13	NW Iran/Caucasus	43,53	41,95	-13,4	-4,7	2,6	-26,7	-2,2	3,1	189%	212%	106%	71%	22%
14	NW Iran/Caucasus	45,59	40,52	-15,3	14,6	167,3	0,0	0,0		0%	0%	1%	1%	0%
15	NW Iran/Caucasus	42,54	40,12	-41,9	21,6	170,2	-27,2	27,2	159,1	82%	72%	36%	24%	7%
16	NW Iran/Caucasus	44,15	38,63	-19,9	20,3	175,5	-14,8	15,8	159,3	76%	44%	79%	55%	20%
17	NW Iran/Caucasus	46,14	38,88	-17,3	33,5	150,5	-1,1	1,1	0,0	4%	3%	2%	98%	52%
18	NW Iran/Caucasus	47,28	37,55	-6,2	24,3	145,6	0,0	0,0		0%	0%	0%	100%	54%
	NW Iran/Caucasus									44%	38%	31%	38%	16%
19	Alborz	49,32	37,44	-7,2	2,6	89,6	-25,1	24,5	75,9	461%	338%	239%	159%	68%
20	Alborz	50,52	36,17	-35,1	20,2	38,8	0,0	0,0		0%	0%	0%	0%	53%
21	Alborz	50,17	35,36	-29,1	8,5	11,4	-17,8	0,6	23,3	59%	60%	30%	20%	17%
22	Alborz	52,39	35,98	-38,6	2,6	24,3	-13,1	0,0	30,0	34%	34%	126%	84%	27%
23	Alborz	52,05	35,17	-29,3	-2,7	169,2	-2,2	0,0	20,0	8%	8%	4%	3%	1%
24	Alborz	53,35	36,37	-28,0	13,2	5,7	-2,9	0,0	169,8	9%	9%	14%	9%	14%
25	Alborz	55,41	35,94	-24,6	4,0	18,3	0,0	0,0		0%	0%	0%	0%	0%
	Alborz									176%	133%	98%	65%	29%
26	Kopet-Dag	56,66	36,66	-12,6	8,1	177,2	-1,7	1,9	153,9	17%	17%	9%	6%	16%
27	Kopet-Dag	58,94	36,57	-16,7	5,5	12,0	-32,4	-0,1	34,9	184%	202%	249%	166%	211%
	Kopet-Dag									97%	105%	123%	82%	109%
28	Lut	56,03	34,77	-18,5	4,3	21,5	-1,5	0,0	33,8	8%	8%	10%	6%	2%
29	Lut	60,34	34,31	-9,2	12,7	32,7	-20,1	19,8	29,6	179%	137%	68%	46%	45%
30	Lut	57,22	32,98	-17,6	-3,7	19,2	-31,2	0,7	42,1	174%	178%	89%	59%	18%
31	Lut	59,03	32,21	-23,6	12,8	37,8	-8,8	8,5	33,8	46%	34%	17%	11%	5%
32	Lut	59,61	29,73	-21,0	29,2	48,0	-9,9	1,3	55,8	28%	28%	23%	15%	5%
33	Lut	57,74	28,81	4,4	28,8	48,0	0,0	0,0		0%	0%	55%	32%	10%
	Lut									72%	62%	33%	22%	13%
34	Central Iran	49,98	34,25	-2,8	2,0	62,4	0,0	0,0		0%	0%	0%	0%	0%
35	Central Iran	52,88	34,04	-14,1	2,8	16,6	0,0	0,0		0%	0%	0%	0%	0%
36	Central Iran	54,49	33,78	-12,2	11,8	2,5	0,0	0,0		0%	0%	0%	0%	0%
37	Central Iran	51,94	32,94	-3,4	1,2	71,3	0,0	0,0		0%	0%	0%	0%	0%
38	Central Iran	53,06	31,59	-13,2	1,2	33,7	0,0	0,0		0%	0%	0%	0%	0%
39	Central Iran	54,83	31,92	-11,9	18,6	12,4	-1,0	1,0	5,0	7%	5%	2%	2%	0%
40	Central Iran	55,93	31,24	-13,4	-2,6	174,6	0,0	0,0		0%	0%	0%	0%	0%
41	Central Iran	55,88	29,55	-7,9	7,1	121,3	-3,8	3,8	43,7	51%	36%	18%	12%	4%
	Central Iran									5%	4%	2%	1%	0%
42	Persian Gulf	50,03	28,46	-6,7	0,1	86,6	0,0	0,0		0%	0%	0%	0%	0%
43	Persian Gulf	51,9	27,34	-1,5	4,2	37,1	0,0	0,0		0%	0%	0%	0%	0%
44	Persian Gulf	53,61	26,43	-17,7	6,4	16,8	0,0	0,0		0%	0%	0%	0%	0%
45	Persian Gulf	55,14	25,33	-1,5	4,3	2,8	0,0	0,0		0%	0%	0%	0%	0%
	Persian Gulf									0%	0%	0%	0%	0%
46	Oman Gulf	57,52	25,14	-128,7	15,0	33,2	0,0	0,0		0%	0%	0%	0%	0%
47	Oman Gulf	59,01	24,83	-69,3	6,6	21,1	0,0	0,0		0%	0%	0%	0%	0%
	Oman Gulf									0%	0%	0%	0%	0%

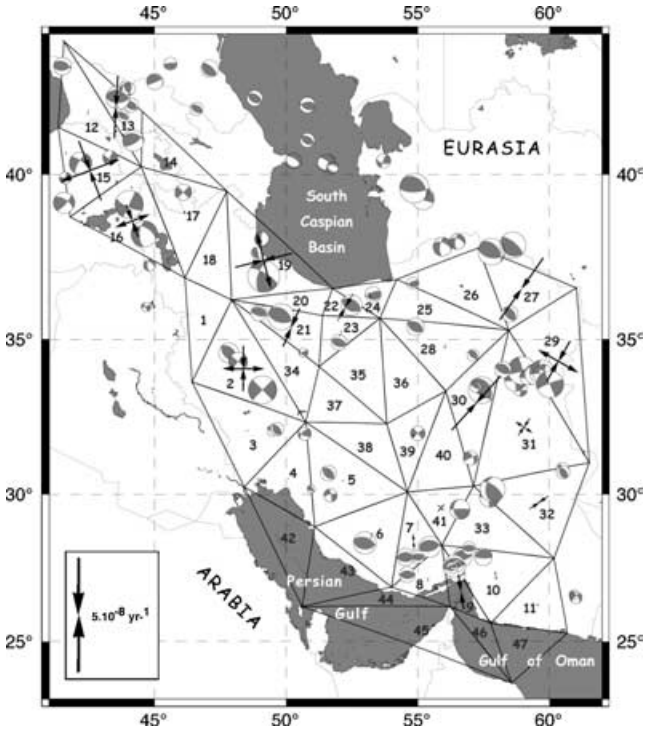

Figure 4. Principal horizontal axes of the seismic strain-rate tensor. The seismic strain-rate tensor is obtained using focal mechanism solutions from Jackson *et al.* (1995) for the time period 1909–1991 completed for the time period 1992–2002 by the Harvard centroid moment tensor catalogue.

than 6.0. Each earthquake was assigned a scalar moment obtained from the catalogues when available or from the continental M_s–M_0 relation of Ekström & Dziewonski (1988). Doing this, we expect to account for most of the seismically released strain for one century. Each triangle may cover zones of different styles of deformation and the Kostrov's summation averages the different styles. Fig. 4 shows the focal mechanisms of the database. A notable contrast is observed between the southern part of Iran (Zagros and Makran ranges) where only small or moderate events occurred and the northern part of Iran (northwest Iran, Talesh, Alborz, Kopet-Dag, northern border of the Lut Block) where large events are observed (Fig. 4 and Table 1, but see also the Fig. 2). For triangle 27, we have included the earthquakes in the Kopet-Dag even if they are located a few kilometres outside the triangle because the GPS site SHIR is located north of the Kopet-Dag.

High seismic strain rates are observed in six zones: (1) the northern borders of the Lut Block, (2) the eastern Kopet-Dag, (3) the central and western Alborz, (4) northwest Iran–eastern Turkey–Caucasus, (5) the Zagros–Makran transition zone and (6) the northern Zagros. For several triangles of the regions 1–4, which correspond to the north and east of Iran, the amplitude of the seismic strain-rate field is of the same order as the amplitude of the geodetic strain-rate field. This could indicate that a large part of the strain is seismic. Conversely, the central and southern Zagros, the Makran, the eastern Alborz and the western Kopet-Dag experience very little seismic deformation while the strain deduced from GPS is large. This could indicate that a large part of the deformation in these regions is aseismic or that the recurrence time of the large events is larger than one century. This will be developed below.

4 COMPARISON OF THE STYLE AND DIRECTION OF THE SEISMIC AND GEODETIC DEFORMATION

Because we use a relatively small earthquake data set, the reliability of the strain computation as a proxy for the long-term seismic strain is questionable. To check this, we perform two tests of similarity of strain-rate patterns of the seismic data over different seismic data sets. In the first test, using the 1909–2002 earthquake database, we sum earthquakes with seismic moment from 10^{18} to 10^{19} N m (small earthquakes, $< M_w$ 6.5) and larger than 10^{19} N m ('large' earthquakes, $> M_w$ 6.5) and compare these patterns together and with the style and orientation of the strain rate inferred from the GPS data. Only a small subset of triangles contains data in these two seismic moment ranges. Therefore the comparison is limited to 11 triangles (Fig. 5a). In most of the triangles the style and the orientation of deformation does not depend of the subset of seismic moment used for computation. There is a good agreement between seismic strain patterns inferred from earthquakes over several intervals of magnitude. Only two triangles show different patterns for the 'large' and 'small' earthquakes. The first one (triangle 2) is located in northern Zagros. Small earthquakes indicate shortening perpendicular to the Zagros range while large earthquakes indicate strike-slip parallel to the Zagros. This is consistent with the partitioning already proposed for the northern Zagros range (Berberian 1995; Talebian & Jackson 2002). As expected, the geodetic strain corresponds to the combination of the large and small earthquake deformations. The second one with discrepancies (triangle 13) is located in the Caucasus. These relatively small earthquakes indicate shortening with a small strike-slip component while large earthquakes indicate pure shortening. We perform a second test dividing the seismicity catalogue into two, separating the earthquakes occurring in the even years and the odd years. The comparison is limited to 12 triangles (Fig. 5b). In all the triangles the style and the direction of the strain-rate tensors are similar. The mean deviation of the direction is less than 2° for both the even- and odd-year cases and the standard deviation of the deviation is about 10°. To summarize, the style and the direction of the seismic strain seems to be well defined for most of the triangles using a time interval of 100 yr.

Fig. 6 shows geodetic and seismic strain-rate axes normalized to the maximum value. This representation allows a comparison of the fix and style of the geodetic and seismic strains even if the seismic strain is small. In most of the triangles the fix and the style of the geodetic and seismic strain rates are similar. This agreement is particularly noticeable in Zagros (triangles 3, 4, 6, 8), Alborz (19, 22, 24) and around the Lut Block (29, 31, 32). In the Zagros, the seismic strain is coaxial with the geodetic strain even if its amplitude is small. This result appears fully consistent with Jackson *et al.* (1995), who proposed that it is possible to accommodate the Arabia–Eurasia motion with simply more deformation of the type revealed by the earthquakes. This consistency between geodetic and seismic strain directions implies that continuum or discontinuous assumptions used to compute style and strain direction lead to the same conclusions (Thatcher 1995). Indeed, geodetic strain corresponds to continuum deformation inside a triangle, and seismic strain is computed with the discontinuous deformation due to displacements along faults. In a few triangles the fix of the seismic and geodetic strain rates is slightly different. Two of these triangles correspond to the triangles discussed in Fig. 5, where the seismic strain deduced from the large and small earthquakes is different. If a triangle includes faults with varied mechanisms, i.e. if the strain is not

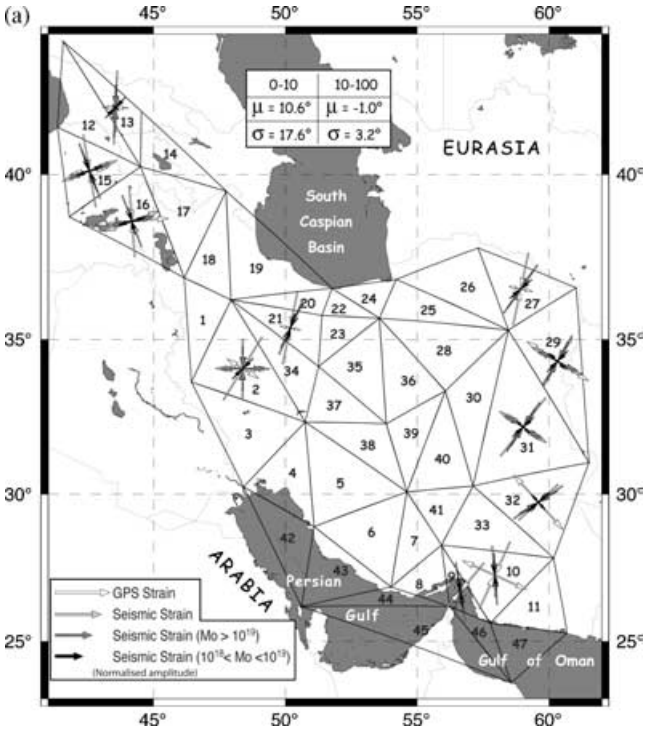

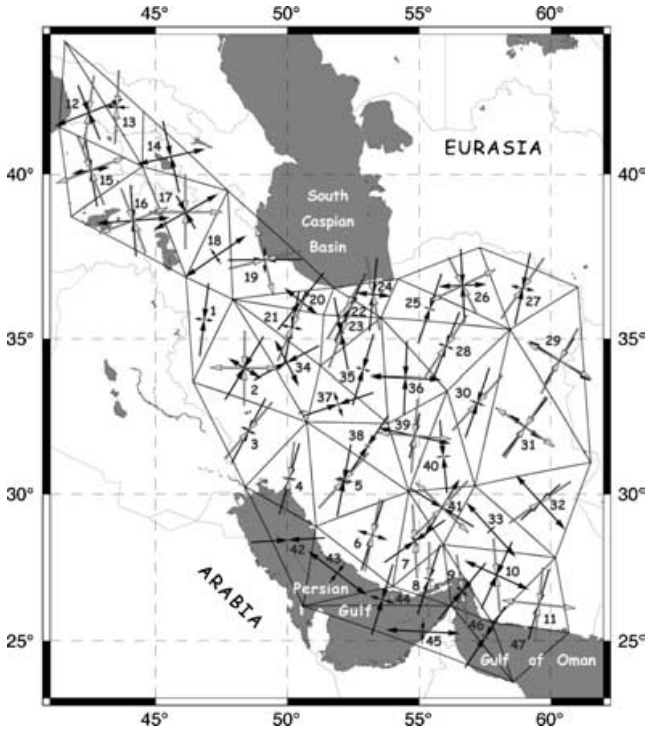

Figure 6. Axes of the geodetic (black arrows) and seismic (grey arrows) strain-rate tensor to compare the direction and style of the seismic and geodetic strain-rate fields. Amplitudes are normalized.

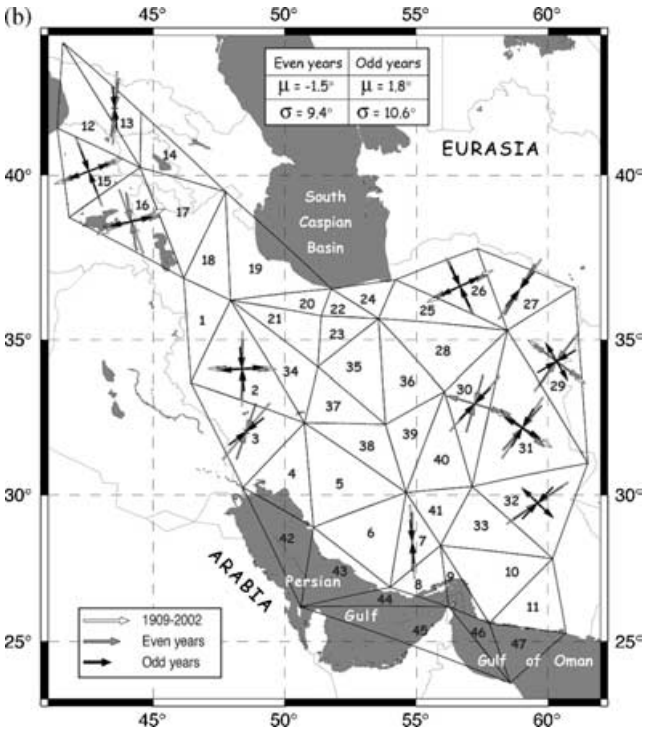

Figure 5. (a) Strain-rate patterns of the seismic data averaged over different seismic moment ranges. Only the styles and the orientations are plotted. Amplitudes are normalized. (b) Strain-rate patterns of the seismic data for the even years and odd years. Amplitudes are normalized. In both figures, the table gives the mean and the standard deviation of the deviation of the direction of the strain obtained using the subsets of data respectively to the whole set of data.

homogeneous in the triangle, and if the studied period does not cover the seismic cycle of all these faults, it is possible to experience local advances or delays in seismic strain release. In this case the direction and style of the strain field that can be deduced from the earthquakes are not statistically reliable.

Summarizing the geodetic and seismic style and direction of deformation, we observe that the southern border of Iran from the Makran to the northern Zagros is characterized by a homogeneous compressive strain orientated N10°. Conversely, northern Iran shows a more complex pattern. This heterogeneity could be due to the existence of the rigid Caspian Block which plays a major role in the tectonic regime of northern Iran, as shown for example by the large velocity contrast between the GPS sites located north of the Alborz range on the southern Caspian shoreline and the GPS site of DAMO, north of the Talesh range (Fig. 1).

5 COMPARISON OF THE RATE OF THE SEISMIC AND GEODETIC DEFORMATION

The main source of uncertainty when one tries to estimate the pattern of the long-term strain rate from earthquake moment tensors is related to the distribution of earthquakes in time. Indeed, a short-duration earthquake catalogue is a random sample of the long-term pattern of seismicity. If the earthquake catalogue spans several recurrence times of large earthquakes, the estimation of the style and of the amplitude of the seismic deformation should be reliable. Otherwise, only the style of the seismic deformation can be determined if the faulting mechanisms are homogeneous as shown in the previous section. The recurrence time of large earthquakes is 250–700 yr along the Tabriz Fault (Berberian & Yeats 1999; Hessami *et al.* 2003) and more than 1000 yr in the Caucasus (Fuenzalida *et al.* 1997). This clearly indicates that the 1909–2002

seismic strain rate can be overestimated or underestimated, depending on the occurrence of earthquakes during the studied time interval relative to the average recurrence interval of large earthquakes. This may imply that the short-term seismic strain-rate field is less stable than the geodetic strain-rate field due to contributions from the largest events leading to local advances or delays in seismic strain release.

The results of Fig. 4 have been obtained using events from 1909 to 2002. To estimate the significance of these results concerning the long-term seismic strain rate, we extend the studied time period using the catalogue of seismicity of Ambraseys & Melville (1982). We compare the results obtained using four time intervals: 1000–2002, 1700–2002, 1800–2002 and 1900–2002 (Fig. 7 and Table 1). Because earthquake mechanisms of historical events are not known, we simply sum the seismic moments and not the seismic tensors (Papazachos & Kiratzi 1996) assuming that the style of deformation remains constant. Doing this we try to obtain a quantitative estimation of the amplitude of the seismic strain rates over a longer time period. For many triangles, this amplitude varies for the four time intervals (Fig. 7) indicating that at local scale a precise estimation of the amplitude of the seismic strain rate needs a more reliable and/or longer historical record of the seismicity. Conversely, computing a mean seismic strain rate for large regions (Zagros, northwest Iran, Alborz and Kopet-Dag/Lut), we obtain a relatively constant mean strain rate for 100, 200 and 300 yr (Table 1). Only the strain rate calculated for the interval 1000–2002 differs markedly. The 1000–2002 period generally indicates lower seismic strain. This is probably due to missing earthquakes for the period 1000–1700 (Ambraseys & Melville 1982). Nevertheless, based on the available catalogues of seismicity, a quantitative estimation of the amplitude of the seismic strain rate at regional scale is possible.

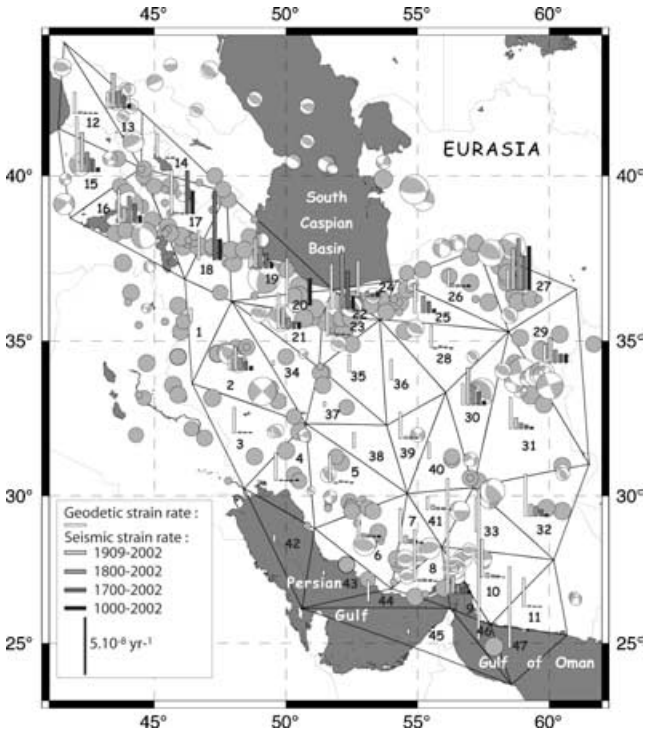

Figure 7. Estimation of the amplitude of the seismic strain rate for the time periods 1000–2002, 1700–2002, 1800–2002 and 1909–2002. The amplitude of the seismic strain rate is obtained using the seismicity plotted on Fig. 2. The amplitude of the geodetic strain rate is indicated in white.

Fig. 7 and Table 1 show that most of the regions experiencing very low seismic strain rates for 1900–2002 (the Central Iranian Block, the central and southern Zagros, the Makran and the western Kopet-Dag) retain very low strain rates whatever the studied interval. Regions with high seismic strain rates for 1909–2002 are more difficult to analyse. In northern Iran and Turkey a high seismic strain is confirmed (central Alborz, Kopet-Dag) or revealed (Tabriz region, eastern Alborz). Around the Lut Block the seismic strain rate decreases on considering a larger historical period. This decrease could be due to the occurrence of clustered events in the 20th century and/or the incompleteness of data relating historical events in these regions. The northern Zagros and the Zagros–Makran transition seem to experience very small seismic strain when a large time period is used.

Overall, the seismic strain rate built from 20th-century events (Fig. 4) indicates that the seismic deformation is large in northern Iran, from the Turkish border to the Lut Block, and small in southern Iran. This contrasting behaviour, based on the 1909–2002 catalogue, is still enhanced using the 1700–2002 and 1000–2002 catalogues (Fig. 7). Using these two databases, the seismic deformation seems to be negligible in southern Iran with respect to the total strain. Therefore, historical seismic strain-rate analysis reinforces the contrast between the southern part of Iran which is more or less aseismically deformed and the northern part of Iran which is seismically deformed. Jackson & McKenzie (1988) proposed less than 15 per cent of seismic deformation in Zagros and between 50 and 100 per cent of seismic deformation in Alborz, Kopet-Dag and eastern Iran. Based on 1000 yr time records, our study leads to a percentage of seismic deformation no greater than 3 per cent in the Zagros and of 30 per cent in Alborz (Table 1). Only the Kopet-Dag and the Tabriz region appear to have a dominant seismic behaviour (50–100 per cent). What is the explanation for this large contrast of behaviour between southern and northern Iran? The obvious first cause, proposed by Jackson & McKenzie (1988), is the very thick (more than 8–10 km) sedimentary coverage of the Zagros, decoupled from the basement by a salt layer at its base. Therefore the vertical thickness of the seismogenic layer is too thin to generate large earthquakes which cannot propagate upwards due to the salt layer. This is confirmed by microseismicity studies in the Zagros (Tatar 2001; Hatzfeld *et al.* 2003) showing that most of the earthquakes occur in a thin layer between a depth of 10 and 14 km beneath the sedimentary coverage. Conversely the seismicity in the Alborz extends from the surface down to 15 km depth (Tatar 2001). Nevertheless, using a seismogenic thickness of 5 km, the seismic strain rate in the Zagros always remains smaller than in northern Iran. A second explanation could be the difference of behaviour of the lithosphere south of the Main Recent Fault. Tomographic models (Bijwaard *et al.* 1998; Maggi *et al.* 2000) show a large contrast in the lithosphere beneath the Main Recent Fault. North of the fault and up to the Caspian Basin the lithosphere between 50 and 100 km depth shows low V_p velocity and high *Sn* attenuation, while beneath the Zagros the velocity is high and the attenuation is low. No obvious physical relation links these observations to the seismic/total deformation ratio. Nevertheless, the geographical correlation is high and must be mentioned.

6 COMPARISON OF THE NUMBER OF EARTHQUAKES AND GEODETIC DEFORMATION

As already shown in Fig. 2(a), although the Zagros is not active in terms of seismic energy it is very active by its number of

earthquakes. The difference in seismic strain rate between north and south appears surprising looking at the number of earthquakes. It has been proposed by Kagan (1999) and Kreemer *et al.* (2002) that there is a strong global correlation between relative geodetic moment rates (between different areas) and the relative number of earthquakes, particularly for subduction zones but also for zones of continental deformation. A qualitative comparison of Figs 2(a) and 3 seems to indicate that this observation is not confirmed at a regional scale in Iran.

Fig. 8 shows geodetic strain rate in each triangle as a function of the number of earthquakes between 1964 and 1999 (for 100 km^2). Three groups of triangles are identified. Group 1 corresponds to the Zagros and is characterized by an intensive seismicity and a high geodetic strain. Group 2, corresponding to central Iran, experiences a low seismicity and no geodetic strain. The last group is in between and suffers low or moderate seismicity but high geodetic strain. It corresponds to the northwest Iran, Alborz, Kopet-Dag and Lut regions. This last group could be split into two subgroups, northwest Iran and Alborz on one side and Kopet-Dag and Lut on the other side, on the basis of the number of earthquakes. The ratio of strain/number of earthquakes is generally higher in the Alborz and northwest Iran than in the Lut and Kopet-Dag.

The seismicity rate in the third group is significantly lower than what is expected given the geodetic strain rate, indicating that the proposition of Kagan (1999) and Kreemer *et al.* (2002) is not verified at regional scale, at least in Iran. Kreemer *et al.* (2002) have observed that the continental areas characterized by major strike-slip faults such as the Altyn Tagh, Saigang and North Anatolian faults suffer a deficit of seismicity in terms of number of earthquakes compared with what is expected based on the geodetic strain rate. Our regional study confirms this observation: all regions of group 3 are crossed by large strike-slip faults. Kreemer *et al.* (2002) proposed that the anomalously low seismicity rate along the major strike-slip faults is caused by the fact that along these fault zones the magnitude–frequency relationship is best approximated by a characteristic earthquake distribution instead of the more general Gutenberg–Richter relationship (Wesnousky 1994). The characteristic earthquake model adequately describes the relatively high occurrence of large events compared with small events.

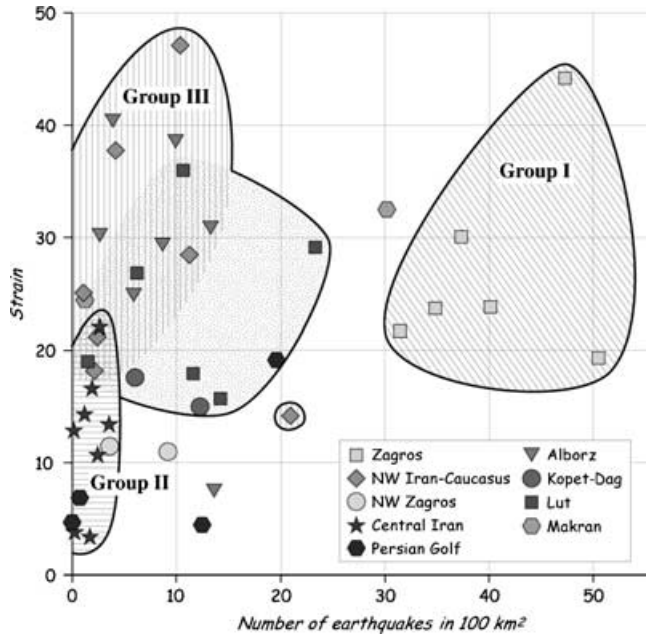

Figure 8. Geodetic strain rate in each triangle given as a function of the number of earthquakes between 1964 and 1999 (per 100 km^2). Three groups of triangles are identified: group 1 = Zagros, group 2 = Central Iran, group 3 = northwest Iran, Alborz, Kopet-Dag, Lut. The third group can be divided in two subgroups: northwest Iran, Alborz and Kopet-Dag/Lut.

7 CONCLUSIONS

Based on the GPS velocity field of Iran (Vernant *et al.* 2004a), we define the quantitative strain pattern of the eastern part of the Arabia–Eurasia collision. The Arabia–Eurasia convergence appears distributed within several regions as mountains belts and large strike-slip faults. The comparison of seismic and geodetic strain rates indicates that highly strained zones experience mainly aseismic deformation in southern Iran (3 per cent seismic) and seismic deformation in northern Iran (30–100 per cent seismic). Spatially, high seismic coupling zones correlates well with high-magnitude earthquake zones. Indeed, intensive but low-magnitude seismicity is observed in the Zagros whereas the largest earthquakes occur in northern and eastern Iran. Compared with Jackson & McKenzie (1988), our study reinforces the contrast between the Zagros and the peri-Caspian belts. These small values represent low but realistic seismic/geodetic ratios. However, the accuracy of historical catalogues is questionable in sparsely populated areas (Ambraseys & Melville 1982). This may explain intermediate values of seismic deformation found in eastern Iran (13 per cent for the 1000–2002 period in the Lut). Therefore, seismic strain analysis may dramatically underestimate the geological strain. By contrast, seismic strain axes seem consistent in direction even with small data sets. We found that seismic strain orientations are often consistent with those deduced from the GPS velocity field. This means that seismic strain can be reliably used to improve geodetic information for the style and the direction of the deformation.

ACKNOWLEDGMENTS

We thank all the participants who helped during the fieldwork in 1999 and 2001. The French Embassy in Tehran contributed to making the experiments successful. The Iran Global GPS project has been sponsored by the French CNRS-INSU 'Intérieur de la Terre' program, the National Cartographic Center (NCC-Tehran) and the International Institute of Earthquake Engineering and Seismology (IIEES-Tehran). A. Kiratsi provided software to compute the seismic strain-rate tensor. This paper benefited from a very constructive and detailed review by Dr Corné Kreemer and an anonymous reviewer. A review by P. Molnar improved the writing of the manuscript. Maps were produced using the public domain Generic Mapping Tools (GMT) software (Wessel & Smith 1995) and with the help of Anne Delplanque.

REFERENCES

Amelung, F. & King, G., 1997. Large-scale tectonic deformation inferred from small earthquakes, *Nature,* **386,** 702–705.

Ambraseys, N.N. & Melville, C.P., 1982. *A History of Persian Earthquakes,* Cambridge University Press, London.

Armijo, R., Hubert, A. & Barka, A., 1999. Westward propagation of the North Anatolian Fault into the northern Aegean: timing and kinematics, *Geology,* **27,** 267–270.

Berberian, M., 1995. Master 'blind' thrust faults hidden under the Zagros folds: active basement tectonics and surface morphotectonics, *Tectonophysics,* **241,** 193–224.

Berberian, M. & King, G.C.P., 1981. Towards a paleogeography and tectonic evolution of Iran, *Can. J. Earth Sci.,* **18,** 210–265.

Berberian, M. & Yeats, R.S., 1999. Patters of historical earthquake rupture in the Iranian plateau, *Bull. seism. Soc. Am.,* **89,** 120–139.

Bijwaard, H., Spakman, W. & Engdahl, E.R., 1998. Closing the gap between regional and global travel time tomography, *J. geophys. Res.,* **103,** 30 055–30 078.

Byrne, D.E., Sykes, L.R. & Davis, D.M., 1992. Great thrust earthquakes and aseismic slip along the plate boundary of the Makran subduction zone, *J. geophys. Res.,* **97,** 449–478.

Ekström, G. & Dziewonski, A.M., 1988. Evidence of bias in the estimation of earthquake size, *Nature,* **32,** 319–323.

Engdahl, E.R., Van der Hilst, R.D. & Buland, R., 1998. Global teleseismic earthquake relocation with improved travel times and procedures for depth determination, *Bull. seism. Soc. Am.,* **88,** 722–743.

Falcon, N.L., 1974. Southern Iran: Zagros mountains, in *Mesozoic–Cenozoic Orogenic Belts,* Geological Society Special Publication 4, ed. Spencer, A. M., pp. 199–211. Geological Society, London.

Fuenzalida, H. *et al.,* 1997. Seismic source study of the Racha-Dzhaya (Georgia) earthquake from aftershocks and broad-band teleseismic body-wave records; an example of active nappe tectonics, *Geophys. J. Int.,* **130,** 29–46.

Hatzfeld, D., Tatar, M., Priestley, K. & Ghafory-Ashtiany, M., 2003. Seismological constraints on the crustal structure beneath the Zagros mountain belt (Iran), *Geophys. J. Int.,* **155,** 403–410.

Hessami, K., Pantosi, D., Tabassi, H., Shabanian, E., Abbassi, M., Feghhi, K. & Sholaymani, S., 2003. Paleoearthquakes and slip rates of the North Tabriz Fault, NW Iran: preliminary results, *Ann. Geophys.,* **46,** 903–915.

Hindle, D., Kley, J., Klosko, E., Stein, S., Dixon, T. & Norabuena, E., 2002. Consistency of geologic and geodetic displacements during Andean orogenesis, *Geophys. Res. Lett.,* **29,** doi:10.1029/2001GL013757.

Holt, W.E., Li, M. & Haines, A.J., 1995. Earthquake strain rates and instantaneous relative motion within central and east Asia, *Geophys. J. Int.,* **122,** 569–593.

Jackson, J.A. & McKenzie, D.P., 1984. Active tectonics of the Alpine-Himalayan Belt between western Turkey and Pakistan, *Geophys. J. R. astr. Soc.,* **77,** 185–264.

Jackson, J.A. & McKenzie, D.P., 1988. The relationship between plate motions and seismic tensors, and the rates of active deformation in the Mediterranean and Middle East, *Geophys. J. R. astr. Soc.,* **93,** 45–73.

Jackson, J.A., Haines, J. & Holt, W., 1994. A comparison of satellite laser ranging and seismicity data in the Aegean region, *Geophys. Res. Lett.,* **21,** 2849–2852.

Jackson, J.A., Haines, J. & Holt, W., 1995. The accommodation of the Arabia-Eurasia plate convergence in Iran, *J. geophys. Res.,* **100,** 15 205–15 219.

Jenny, S., Goes, S., Giardini, D. & Kahle, H.-G., 2004. Earthquake recurrence parameters from seismic and geodetic strain rates in the eastern Mediterranean, *Geophys. J. Int.,* **157,** 1331–1347.

Kagan, Y.Y., 1999. Universality of the seismic moment-frequency relation, *Pure Appl. Geophys.,* **155,** 537–573.

Kostrov, B., 1974. Seismic moment and energy of earthquakes and seismic flow of rock, *Izv. Acad. Sci. USSR, Phys. Solid Earth,* **1,** 23–40.

Kreemer, C., Holt, W.E., Goes, S. & Govers, R., 2000. Active deformation in eastern Indonesia and the Philippines from GPS and seismicity data, *J. geophys. Res.,* **105,** 663–680.

Kreemer, C., Holt, W.E. & Haines, A.J., 2002. The global moment rate distribution within plate boundary zones, in *Plate Boundary Zones,* AGU Geodynamics Series 30, ed. Stein, S. & Freymueller, J.T., pp. 173–190, American Geophysical Union, Washington, DC.

Kreemer, C., Holt, W.E. & Haines, A.J., 2003. An integrated global model of present-day plate motions and plate boundary deformation, *Geophys. J. Int.,* **154,** 8–34.

Maggi, A., Jackson, J.A., Priestley, K. & Baker, C., 2000. A re-assessment of focal depth distributions in southern Iran, the Tien Shan and northern India; do earthquakes really occur in the continental mantle?, *Geophys. J. Int.,* **143,** 629–661.

Malvern, L.E., 1969. *Introduction to the Mechanics of a Continuum Medium,* Prentice-Hall, Englewood Cliffs, NJ.

Masson, F. *et al.,* 2004. A GPS network to monitor continental deformation in NW Iran—consequences on the seismic hazard along the Tabriz fault, *Geophysical Research Abstract,* Volume 6, EGU General Assembly 2004, Abstract number EGU04-A-01384.

McCaffrey, R., 1997. Statistical significance of the seismic coupling coefficient, *Bull. seism. Soc. Am.,* **87,** 1069–1073.

McClusky, S. *et al.,* 2000. Global Positioning System constraints on plate kinematics and dynamics in the eastern Mediterranean and Caucasus, *J. geophys. Res.,* **105,** 5695–5719.

Nilforoushan, F. *et al.,* 2003. GPS network monitors the Arabia–Eurasia collision deformation in Iran, *J. Geod.,* **77,** 411–422.

Papazachos, C. & Kiratzi, A., 1992. A formulation for reliable estimation of active crustal deformation and its application to central Greece, *Geophys. J. Int.,* **111,** 424–432.

Papazachos, C. & Kiratzi, A., 1996. A detailed study of the active crustal deformation in the Aegean and surrounding area, *Tectonophysics,* **253,** 129–153.

Shen-Tu, B., Holt, W.E. & Haines, A.J., 1998. The contemporary kinematics of the western United States determined from earthquake moment tensors, very long baseline interferometry, and GPS observations, *J. geophys. Res.,* **103,** 18 087–18 117.

Shen-Tu, B., Holt, W.E. & Haines, A.J., 1999. Deformation kinematics in the western United States determined from Quaternary fault slip rates and recent geodetic data, *J. geophys. Res.,* **104,** 28 927–28 955.

Straub, C., Kahle, H.-G. & Schindler, C., 1997. GPS and geologic estimates of the tectonic activity in the Marmara Sea region, NW Anatolia, *J. geophys. Res.,* **102,** 27 587–27 601.

Talebian, M. & Jackson, J.A., 2002. Offset of the Main Recent Fault of NW Iran and implications for the late Cenozoic tectonics of the Arabia–Eurasia collision zone, *Geophys. J. Int.,* **150,** 422–439.

Talebian, M. & Jackson, J.A., 2004. A reappraisal of earthquake focal mechanisms and active shortening in the Zagros mountains of Iran, *Geophys. J. Int.,* **156,** 506–526.

Tatar, M., 2001. Etude sismotectonique de deux zones de collision continentale: le Zagros central et l'Alborz (Iran), *PhD thesis,* University of Grenoble, Grenoble.

Thatcher, W., 1995. Microplate versus continuum descriptions of active tectonic deformation, *J. geophys. Res.,* **100,** 3885–3894.

Vernant, P. *et al.,* 2004a. Contemporary crustal deformation and plate kinematics in middle east constrained by GPS measurement in Iran and northern Oman, *Geophys. J. Int.,* **157,** 381–398.

Vernant, P. *et al.,* 2004b. Deciphering oblique shortening of central Alborz in Iran using geodetic data, *Earth plant. Sci. Lett.,* **223,** 177–185.

Wang, Q. *et al.,* 2001. Present-day crustal deformation in China by Global Positioning System measurements, *Science,* **294,** 574–577.

Ward, S., 1990. Pacific–North America plate motions: new results from very long baseline interferometry, *J. geophys. Res.,* **95,** 21 965–21 981.

Wesnousky, S.G., 1994. The Gutenberg–Richter or characteristic earthquake distribution, which is it?, *Bull. seism. Soc. Am.,* **84,** 1940–1959.

Wessel, P. & Smith, W.H.F., 1995. New version of the generic mapping tools released, *EOS, Trans. Am. geophys. Un.,* **76,** 329.